

International Journal of Pharmacology

ISSN 1811-7775





ISSN 1811-7775 DOI: 10.3923/ijp.2025.429.442



Research Article Design, Synthesis Optimization and Anticancer Activity of Small Molecule Kinase Inhibitors

¹Jialiang Sun, ²Tong Li, ¹Xi Chen, ³Cheng Peng, ¹Lu Liu, ¹Baorong Hu and ¹Shuang Zhao

Abstract

Background and Objective: The development of inhibitors targeting protein kinases (PKs) has emerged as a pivotal field in drug research. In this context, a comprehensive analysis of kinase structural attributes has led to the proposal of a pyrimidine-linked biphenyl core (PBC) pharmacophore model aimed at bridging the adenine-binding region and the hydrophobic pocket left vacant by the DFG segment rotation. Materials and Methods: Building upon this, a Suzuki One-Pot Reaction was employed to synthesize 20 derivative compounds, among which F1 and F2 exhibited heightened tumor inhibitory potential (IC_{50} <10 μ M). These synthesized compounds were subjected to a Thiazolyl Blue (MTT) assay to assess their impacts on cell proliferation. Meanwhile, the in vivo anticancer effects were validated through rat tumor xenograft experiments. Immunofluorescence staining of tumor tissues in rats was utilized to observe DNA damage and cell apoptosis. Additionally, liver and kidney tissues were subjected to Hematoxylin-Eosin (H&E) staining to evaluate the influence of the inhibitors on rat liver and kidney cells. **Results:** The pronounced antiproliferative capabilities of F1 and F2 against tumor cells, while exerting minimal influence on normal human cells, indicating substantial tumor cell-selective toxicity (p < 0.001). After 24 hrs of exposure to F1 and F2, a notable increase in tumor cell apoptosis was observed, with MTT assays showing an IC₅₀ of 2.9 μm for F1 and 8.0 μm for F2, signifying significant tumor cell inhibition. Compared to the control (Ctrl) group, the levels of γH2AX signal and relative protein expression in the F1 and F2 group were significantly higher (p<0.001). However, there were no significant toxic side effects observed in the rat liver and kidney tissues (p>0.001). **Conclusion:** In summary, the PBC pharmacophore model opened novel avenues for developing relevant drugs for PK inhibitors. In the future, compound design and optimization based on this model hold promise for delivering new effective drugs for diseases like cancer.

Key words: Small molecule kinase inhibitors, protein kinase, X-ray crystallography, antitumor activity, protein kinases, pyrimidine-linked biphenyl

Citation: Sun, J., T. Li, X. Chen, C. Peng, L. Liu, B. Hu and S. Zhao, 2025. Design, synthesis optimization and anticancer activity of small molecule kinase inhibitors. Int. J. Pharmacol., 21: 429-442.

Corresponding Author: Shuang Zhao, Department of Pharmacy, The First Affiliated Hospital of Harbin Medical University, Harbin, 150001, China

Funding: This work was supported by Research Projects of Heilongjiang Provincial Health Commission (2019-008 and 2020-147).

Copyright: © 2025 Jialiang Sun *et al.* This is an open access article distributed under the terms of the creative commons attribution License, which permits unrestricted use, distribution and reproduction in any medium, provided the original author and source are credited.

Competing Interest: The authors have declared that no competing interest exists.

Data Availability: All relevant data are within the paper and its supporting information files.

¹Department of Pharmacy, The First Affiliated Hospital of Harbin Medical University, Harbin, 150001, China

²Prenatal Diagnosis Center, The First Affiliated Hospital of Harbin Medical University, Harbin, 150001, China

³School of Biological and Pharmaceutical Engineering, Jilin Agricultural Science and Technology University, Jilin, 132101, China

INTRODUCTION

Protein kinases (PKs), also referred to as protein phosphate kinases, constitute a crucial class of enzymes responsible for catalyzing protein phosphorylation reactions. They play a pivotal role in regulating and transmitting various physiological signals within cell¹. The PKs modulate intracellular signaling pathways by transferring phosphate groups to specific substrate proteins, thereby participating in biological processes^{2,3}. Under normal cellular physiological conditions, the activity of PKs is rigorously controlled to maintain intracellular homeostasis. However, aberrant activation or overexpression of PKs can disrupt cell signaling pathways, promoting phenomena such as proliferation, metastasis and drug resistance in cancer cells. This can subsequently lead to the onset and progression of diverse diseases, including cancer⁴⁻⁶.

The PK inhibitors represent a class of compounds capable of intervening in the activity of PKs. They achieve this by selectively binding to PKs, thereby impeding their activity and regulating the transmission of cellular signaling pathways^{7,8}. The PK inhibitors have garnered significant attention in the field of drug development, particularly playing a pivotal role in the study of anticancer drugs9. The PK inhibitors can be categorized based on their mode of binding. Type I inhibitors complex with the kinase's active conformation within the adenosine triphosphate (ATP) binding site¹⁰. They can interchange with ATP and are therefore referred to as ATPcompetitive inhibitors. However, due to the considerable similarity of various kinases in the ATP-binding region, the selectivity of type I inhibitors is often suboptimal^{11,12}. Type II inhibitors, on the other hand, bind to non-ATP binding pocket sites on the kinase. They occupy both the adenine region of ATP and the new binding pocket formed by the rotation of the activation loop. This induction and stabilization of a kinase's altered conformation leads to kinase inactivation, earning them allosteric inhibitors 13,14. Owing to the distinct nature of their binding sites on the kinase, this class of compounds exhibits higher selectivity. The approved drug imatinib, for example, serves as an allosteric inhibitor of the Bcr/Abl kinase¹⁵.

The Suzuki One-Pot Reaction, also known as the multicomponent Suzuki coupling reaction, is a significant method in organic synthesis widely employed for constructing carbon-carbon bonds¹⁶. This technique utilizes palladium catalysts to couple aromatic compounds containing aromatic bromides or iodides with aromatic compounds containing organic boron reagents, resulting in the formation of new bonds¹⁷. This coupling reaction is characterized by its

efficiency, high selectivity and broad substrate applicability, making it extensively utilized in the field of drug development, especially in the synthesis of Small Molecule Kinase Inhibitors (SMKIs)^{18,19}.

This research was to thoroughly analyze the structural characteristics of PKs, leading to the proposal of a novel pharmacophore model centered around a pyrimidine-linked biphenyl core (PBC). This pharmacophore model aimed to bridge the adenine-binding region of PKs and the hydrophobic cavity created by the rotation of the DFG segment, thereby offering new possibilities for the chemical modification of PK inhibitors. The research also involved the utilization of the Suzuki One-Pot Reaction to synthesize a series of derivative compounds, which were subjected to comprehensive in vitro and in vivo activity evaluations. By synthesizing and analyzing these compounds. This research was intended to yield robust evidence for the design and optimization of future PK inhibitors, consequently offering new and effective drug options for the treatment of diseases like cancer. Through this research, it was hoped that a deeper understanding of PKs in diseases and development of more potent anticancer drugs can be achieved, ultimately contributing to the improvement of survival and quality of life of the patients.

MATERIALS AND METHODS

Study area: This experiment was conducted in The First Affiliated Hospital of Harbin Medical University from December, 2022 to July, 2023.

Design idea and product synthesis: Based on the X-ray crystal structures of kinases and the published concepts of kinase conformational inhibitors, a design was envisaged with a six-membered aromatic heterocycle as the A ring and a fused heterocycle as the B ring to explore the structural and hydrogen bonding features in this region, as well as the distance between R1 and R2 and the relative pharmacophore conformation, as depicted in Fig. 1a. By altering the substituents R1 and R2 on the pharmacophore or introducing structural fragments from molecules with reported kinase activity, the design and synthesis of conformational inhibitors for other kinases were achieved. In various known kinase conformational states, the binding site of R2 is a hydrophobic cavity. Therefore, for most active compounds, R2 is an alkyl or aryl group-substituted amide²⁰. By replacing R2 with fused aromatic heterocycles, the molecule can be extended into the adenine-binding region previously complexed by the adenine of adenosine triphosphate. These heteroaromatic substituents

Fig.1(a-d): Design strategy and synthetic pathways for SMKIs, (a) Design of novel SMKIs, (b-c) Synthesis processes for pathway 1 and pathway 2, respectively and (d) Structural diagrams of the novel kinase conformational inhibitors, F1 and F2

can be probes for exploring hydrogen bonding, polar and hydrophobic surfaces, thereby selecting and inducing kinase conformational states with the corresponding structural features in this region.

Based on the aforementioned information, the design of the corresponding compound series was accomplished through two distinct synthetic pathways. The specific experimental steps involved dissolving the precursor intermediates in methanol (Sigma, USA), subsequently adding the catalyst Pb/C (Sigma, USA) under hydrogen gas conditions and maintaining a certain pressure in the system. After stirring the reaction for 6 hrs, EDCI (Aladdin Reagent Company Limited, China) and DMAP (Aladdin Reagent Company Limited, China) were introduced for the reaction, resulting in the formation of compound (3). The pyrimidine-linked biphenyl-like compounds were synthesized using the Suzuki One-Pot Reaction. Bromonitrobenzene (Sigma, USA) and bis-pinacolato diboron (Sigma, USA) were refluxed with potassium acetate (Sigma, USA) and bis(diphenylphosphine) ferrocene (Sigma, USA) for 18 hrs, followed by the addition of pyrimidine compounds to obtain the intermediate (7). Subsequent addition of p-toluenesulfonic acid (Sigma, USA) initiated a substitution reaction, concluding the derivatization of the scaffold. Detailed synthetic procedures for pathway 1 and pathway 2 were illustrated in Fig. 1(b-c), respectively.

The 20 synthesized compounds were subjected to a simple MTT assay, resulting in the identification of two compounds, F1 and F2, which exhibited high yields and potent inhibition of tumor cell activity (IC $_{50}$ <10 μ M). These compounds were labeled as shown in Fig. 1d-(15) and (16).

Cell culture

Cell revival: The cryopreserved cell samples were retrieved from a -80°C freezer (Siemens, Germany) and swiftly transferred into a 37°C water bath (Thermo Fisher Scientific, USA) within a BBS-DDC clean bench (Shandong Boke Scientific Instrument Co., Ltd., China) or centrifuged in a KH19A centrifuge (Hunan Kaida Scientific Instrument Co., Ltd., China). This ensured quick thawing of the cells. The thawed cells were transferred to a 50 mL centrifuge tube (Greiner Bio-One, Austria), where a small amount of culture medium was added. Centrifugation was implemented at 1,200 rpm for 5 min. Following supernatant removal, 10 mL of culture medium was mixed, mixed thoroughly and the culture vessel was sealed. The containers were placed inside a 37°C 371 CO₂ cell culture incubator (Thermo Fisher Scientific, USA) to maintain a constant temperature and provide the necessary temperature and environmental conditions for cell growth.

Cell passaging: Once the cell density reached a certain level (80-90%), the culture medium and cell waste in the culture dish were discarded. Then, a cell detachment solution containing enzymes like trypsin (Gibco, USA) was added and the specimens were rinsed five times with 1 mL of phosphate-buffered saline (PBS) (Sigma, USA) and subsequently immersed in 2 mL of trypsin substitute. Cell contraction was observed under the SZ61 inverted fluorescence microscope (Olympus, Japan), following which the cells were detached from the culture dish. The detached cells were seeded onto new sterile culture dishes at a 1:3 ratio, thoroughly dispersed and provided with fresh culture medium. The dishes were then positioned in a CO_2 incubator (Thermo Fisher Scientific, USA) at 37°C for consistent temperature cultivation.

Apoptosis detection: The HepG2 liver cancer cells (Shanghai Kelei Biotechnology Co., Ltd., China) were evenly seeded at a density of 1×10⁵ cells per well in a 6-well plate (Thermo Fisher Scientific, USA). The corresponding experimental compounds F1 group, F2 group and control group were added. Subsequently, they were cultured all the night at 37°C in a CO₂ incubator. Each well was diluted with 1 mL of 10% Dulbecco's Modified Eagle Medium (DMEM) culture medium (Sigma, USA) culture medium. After washing with PBS or enzyme-free buffer to remove serum and other substances from the culture medium, 100 µL of Annexin V and PI fluorescent dyes (Sigma, USA) were added to mark apoptotic cells, with the mixture being gently mixed. After a 30 min incubation period under low-temperature and light-protected conditions, the fluorescence and scatter signals of the cells were measured using the Accuri C6 flow cytometer (BD Bioscience, USA). Quantitative and qualitative analyses were performed on the cells to assess the extent of apoptosis.

Animal experiments: Thirty male BALB/c-Nude mice with Specific Pathogen-Free (SPF) status were selected from Chengdu Dashuo Experimental Animal Co., Ltd., China. The mice were aged between 3-4 weeks and weighed approximately 10-15 g. The mice were maintained under standard laboratory conditions, including temperature $(23\pm2^{\circ}\text{C})$, humidity $(50\pm5\%)$, 12 hrs light-dark cycle with dim light, good ventilation and noise levels below 80 decibels. Before the experiments, the mice were acclimated to these conditions for 1 week. They were subjected to fasting for 12 hrs and water deprivation for 6 hrs prior to the procedure.

Ethical consideration: The experimental protocol was approved by Animal Ethical Committee of The First Affiliated Hospital of Harbin Medical University (ethical approval no.

2020147). All the experimental protocols involved in the current investigation followed the Guide for the Care and Use of Laboratory Animals of the National Institutes of Health and the ARRIVE (Animal Research: Reporting of *in vivo* Experiments) guidelines.

Anticancer activity of novel SMKIs

MTT assay: The MTT assay was a commonly used method for assessing cell proliferation and cytotoxicity²¹. The MTT reagent was reduced by viable cells to form a purple product, which can be quantified by measuring its absorbance. This allowed for the evaluation of cell viability and proliferation status.

Logarithmic phase cells were collected and seeded at 7×10^3 cells per well. They were subjected to a CO $_2$ incubation at $37\,^{\circ}$ C all night, with three replicate wells set for each group. Then, 20 μ L of MTT solution (5 mg/mL) (Gibco, USA) was added to each well for a 4 hrs cell culture. Following this, the plates were placed in a centrifuge (1,000 rpm, 10 min) to remove the supernatant. Subsequently, 100 μ L of Dimethyl Sulfoxide (DMSO) (Sigma, USA) was added to each well, followed by gentle agitation on a shaker for 10 min to ensure thorough dissolution. The absorbance values of each well were then measured at OD 490 nm using the HBS-1096C microplate reader (Nanjing Dedier Experimental Equipment Co., Ltd., China). Furthermore, cell viability was quantified based on the tumor cell survival rate (SR).

Tumor xenograft experiment: The HepG2 tumor xenografts were subcutaneously implanted into the dorsal skin of mice. Once the tumor volume was 150 mm³, 30 mice were randomly grouped into three, each containing 10 mice: F1 group, F2 group and control (Ctrl) group. In the F1 group, mice were orally administered F1 at 10 mg/kg/day. Similarly, in the F2 group, mice were given F2 at 10 mg/kg/day. In contrast, the Ctrl group received an equivalent volume of physiological saline. Oral gavage was performed once daily. The treatment was administered continuously for 14 days, during which the tumor volume was measured every two days.

Preparation of drug formulation: The corresponding solvent was dissolved in a water solution with 5% DMSO, 30% polyethylene glycol 300 (Sigma, USA) and 10% polysorbate 80 (Sigma, USA).

After treatment, mice were euthanized using cervical dislocation to dissect their tumor tissues and collect their liver and kidney tissues. These tissues were then placed in a 4% solution of soluble polytetrafluoroethylene (PFA) (Tetrafluoro New Materials Co., Ltd.) and stored at low temperatures for future use.

Immunofluorescence staining

Immunofluorescence staining of tumor tissues from HepG2

cells: They were subjected to immunofluorescence staining. These tissues were fixed on ice for 4 hrs to preserve their morphological structure and protein stability. Fixed tissue samples were dehydrated using a series of increasing concentrations of ethanol solutions to remove water content. Then, a clearing agent (xylene) (Gibco, USA) was used to render the samples transparent. The samples were then immersed in melted paraffin wax (58°C, 2 hrs) for even infiltration. Afterward, the tissue samples were processed with liquid nitrogen and subjected to frozen sectioning to obtain thin slices of tumor tissue.

Immunofluorescence staining of phosphorylated histone

H2AX (γ**H2AX**): It is a commonly used experimental method to assess the extent of DNA double-strand breaks and DNA damage. Firstly, tissue sections were prepared and antigen retrieval was performed using an antigen retrieval buffer (glycine-tris-ethylenediaminetetraacetic acid buffer, Tris-EDTA) (Thermo Fisher Scientific, USA) to enhance the binding efficiency of the antibody to γH2AX. Subsequently, a secondary antibody labeled with a fluorophore (DAPI) (Sigma-Aldrich, USA) was utilized to bind to the primary antibody, thereby tagging the fluorescent signal to the γH2AX protein. Finally, the specimens were observed using a fluorescence microscope to detect the fluorescent signal of γH2AX and to further examine the morphology of the cell nuclei.

Western blotting (WB): After collection of tumor tissues, they were ground and centrifuged to collect the supernatant, followed by another centrifugation step to remove cellular debris. Subsequently, protein extraction buffer (from Gibco, USA) was added and after dissolution, centrifugation was performed to precipitate cellular debris and collect the supernatant. Protein concentration was determined using a protein assay kit (obtained from Shanghai Enzyme-linked Biotechnology Co., Ltd., China). Equal amounts of protein were subjected to Sodium Dodecyl Sulfate-Polyacrylamide Gel Electrophoresis (SDS-PAGE) using gels from Sigma-Aldrich (USA) and then transferred onto Polyvinylidene Difluoride (PVDF) membranes (from R&D, USA). After thorough incubation, the membranes were incubated with a solution containing 5% skim milk powder (from Gibco, USA) and then shaken. Subsequently, diluted anti-yH2AX antibodies (from EBioscience, USA) were added and allowed to incubate overnight, followed by washing with TBST buffer. Following that, HRP- HRP-conjugated anti-rabbit IgG (from Gibco, USA) was added and incubated for 1-2 hrs followed by washing. Subsequently, chemiluminescence was used to detect the signal of the target protein _YH2AX on the membrane. Chemiluminescence detection (from Shanghai Enzyme-linked Biotechnology Co., Ltd., China) was utilized to visualize the bands and digital imaging analysis software was employed to scan the density of the electrophoresis bands. The relative expression levels of γ H2AX were quantitatively analyzed using β -actin as an internal reference.

H&E staining: Mouse liver and kidney tissues were carefully extracted and washed with pre-chilled PBS buffer. The tissues were then fixed using 4% paraformaldehyde (Gibco, USA) and left to fix at room temperature for 24 hrs. After fixation, a gradient dehydration process was carried out, gradually immersing the tissues in ethanol solutions to remove water content. The myocardial tissues were embedded in paraffin and sectioned into 5 µm-thick slices using the CM1950 cryostat (Leica Biosystems, Germany). Subsequently, the sections were deparaffinized and stained using the Hematoxylin and Eosin (H&E) staining kit (from Beijing Solarbio Technology Co., Ltd., China). Dehydration and clearing were achieved by treating the sections with ethanol solutions. The prepared sections were then placed on microscope slides for observation and assessment using a microscope (Leica Microsystems, Germany).

Statistical analysis: All biochemical and cellular experiments were performed in triplicate. Data processing was conducted using SPSS 26.0. Quantitative data were presented as Mean \pm Standard Deviation. For multiple-group comparisons, a one-way analysis of variance was utilized, while for comparisons between two groups, a t-test was employed. Categorical data were presented as frequencies or rates and inter-group comparisons were conducted using the χ^2 test. The p<0.05 was considered statistically significant.

RESULTS

Tumor cell apoptosis: Flow cytometry was used to detect the apoptosis of HCC827 and HepG2 cells. Figure 2(a-d) and Fig. 3(a-d) show the apoptosis of HCC827 and HepG2 cells in the control group, respectively. Figure 2b and 2e, as well as Fig. 3b and 3e, respectively, show the apoptosis of HCC827 and HepG2 cells treated with F1 and F2 for 24 hrs. After 24 hrs, some tumor cells begin to apoptosis (t) until 48 hrs (Fig. 2c and 2f, Fig. 3c and 3f) and massive tumor cells show apoptosis. The upper left corner of the image represents early apoptosis, the lower left corner represents late apoptosis and the lower right corner represents cell necrosis. The results showed that after adding F1 and F2 for 48 hrs, the proportion of apoptosis to healthy cells significantly increased.

Based on the above cell apoptosis results, the apoptosis results were statistically analyzed. The results showed that F1 and F2 can significantly induce tumor cell apoptosis after 24 hrs, achieving their anticancer effect. Figure 4(a-b) show that the proportion of Annexin V+ in HCC827 tumor cells treated with F1 and F2 was significantly higher than that at 0 hr (p<0.01); Fig. 4(c-d) show that the proportion of Annexin V+ in HepG2 tumor cells treated with F1 and F2 was significantly higher than that at 0 hr (p<0.01).

Toxicity results: The expression levels of F1 (Fig. 5a) and F2 (Fig. 5b) in HepG2 tumor cells were evaluated. Experimental results showed that the IC₅₀ values for F1 and F2 were 2.9 and $8.0 \mu m$, respectively, both less than $10 \mu m$.

Specific killing effect of the compound on tumor cells: Further investigation compared the cell viability after 24 hrs of treatment with F1, F549, HCC827 and HepG2 cells. The outcomes showed that F1 and F2 exhibited varying degrees of cytotoxicity on A549, HCC827 and HepG2 cells, leading to a great decrease in cell viability after 24 hrs (p<0.05), which remained 40-70%. However, no observable cytotoxicity was visualized on NCM460 cells (p>0.05), specific data can be found in Fig. 6.

Effects of compounds on tumor cells in vivo: After performing tumor xenograft transplantation in mice, a 14-day continuous treatment regimen was initiated and tumor tissue volume was measured every two days. When the treatment was completed, all mice were euthanized to collect and weight their tumor tissues. The results showed that compared with the Ctrl group, the tumor tissue weight of the F1 and F2 groups was significantly lower (p<0.001) (Fig. 7a). In addition, compared with the Ctrl group, the tumor tissue volume of mice treated with F1 and F2 groups was significantly smaller (p<0.001) (Fig. 7b).

Results of immunofluorescence staining of tumor tissue: Immunofluorescence staining was performed on isolated tumor tissues. The results revealed a significant increase in γ H2AX signal in the immunofluorescence staining images of the F1 and F2 group compared to the Ctrl group. Figure 8 shows the immunofluorescence staining images.

WB detection results: The results of the WB analysis conducted on isolated tumor tissues indicated a significantly higher relative protein expression level of γ H2AX in the F1 and F2 group compared to the Ctrl group (p<0.001) (Fig. 9a). Figure 9b shows the WB detection results.

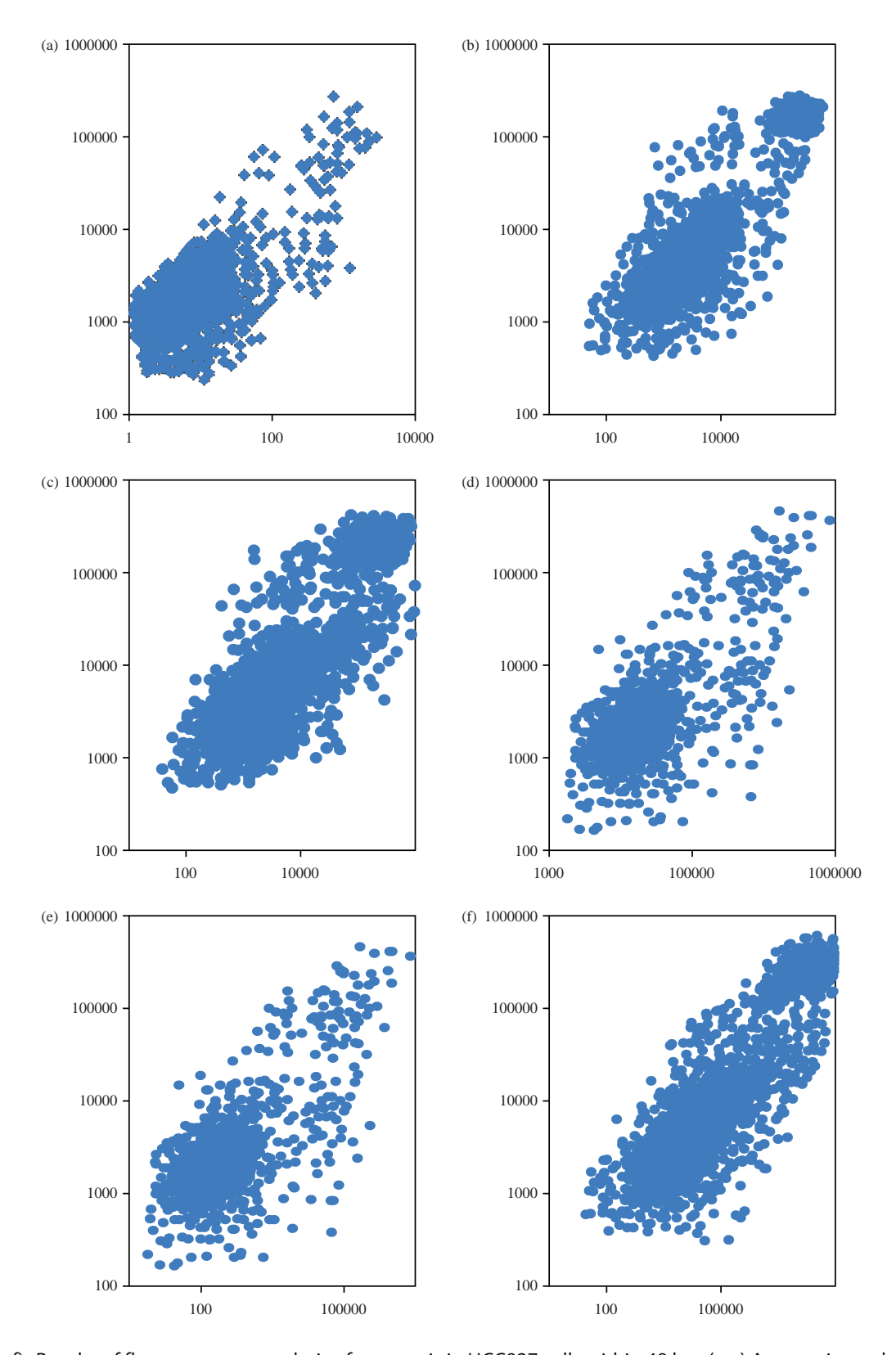


Fig. 2(a-f): Results of flow cytometry analysis of apoptosis in HCC827 cells within 48 hrs, (a-c) Apoptosis results of HCC827 cells in Ctrl group, 24 hrs after F1 treatment and 48 hrs after F1 treatment, respectively and (e-f) Apoptosis results of HCC827 cells in Ctrl group, 24 hrs after F2 treatment and 48 hrs after F2 treatment, respectively

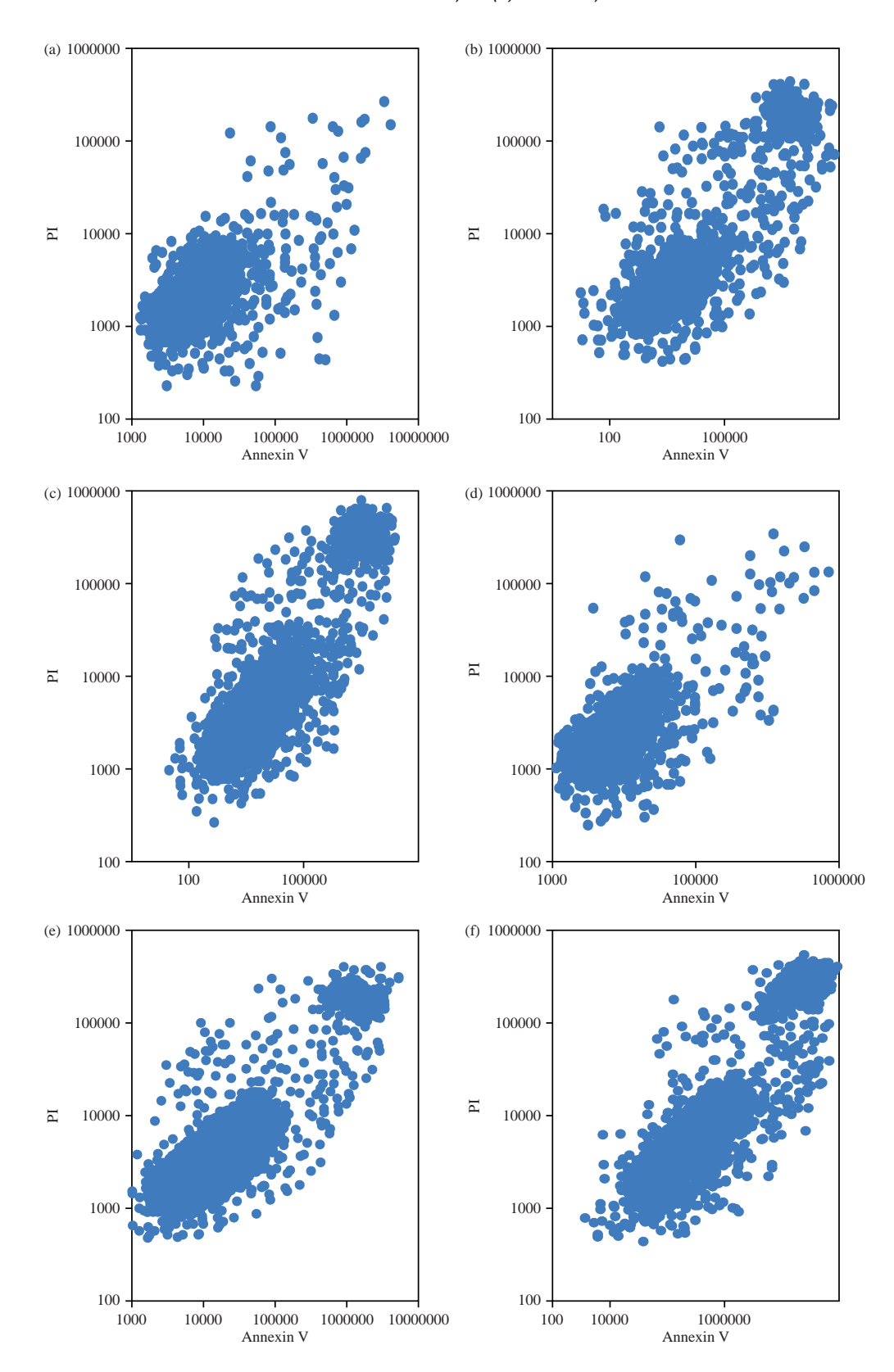


Fig. 3(a-f): Results of flow cytometry analysis of apoptosis in HepG2 cells within 48 hrs, (a-c) Apoptosis results of HepG2 cells in Ctrl group, 24 hrs after F1 treatment and 48 hrs after F1 treatment, respectively and (e-f) Apoptosis results of HepG2 cells in Ctrl group, 24 hrs after F2 treatment and 48 hrs after F2 treatment, respectively

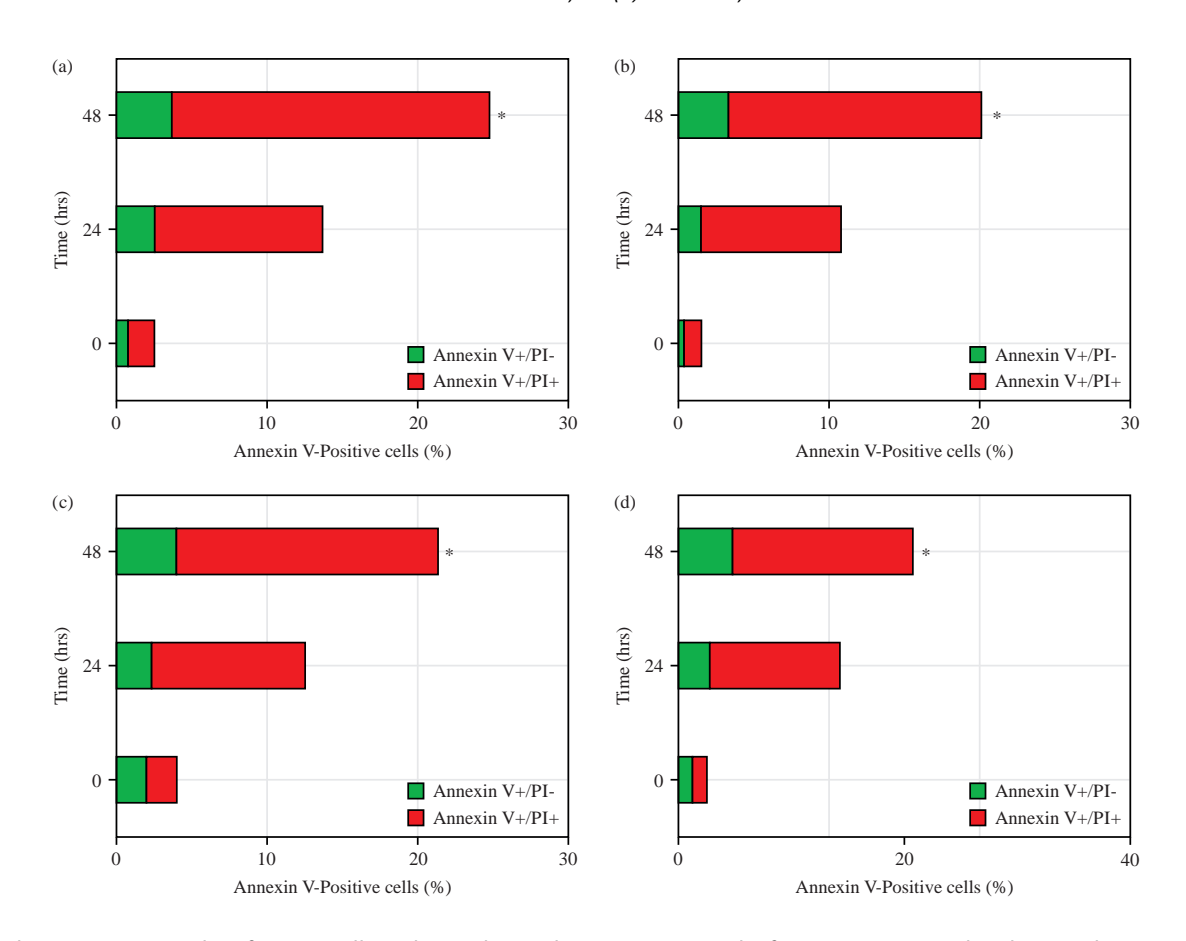


Fig. 4(a-d): Apoptosis results of tumor cells within 48 hrs, (a-b) Apoptosis results for HCC827 treated with F1 and F2, respectively and (c-d) Apoptosis results for HepG2 treated with F1 and F2, respectively

*Compared with the conditions at 0 hr and p<0.05

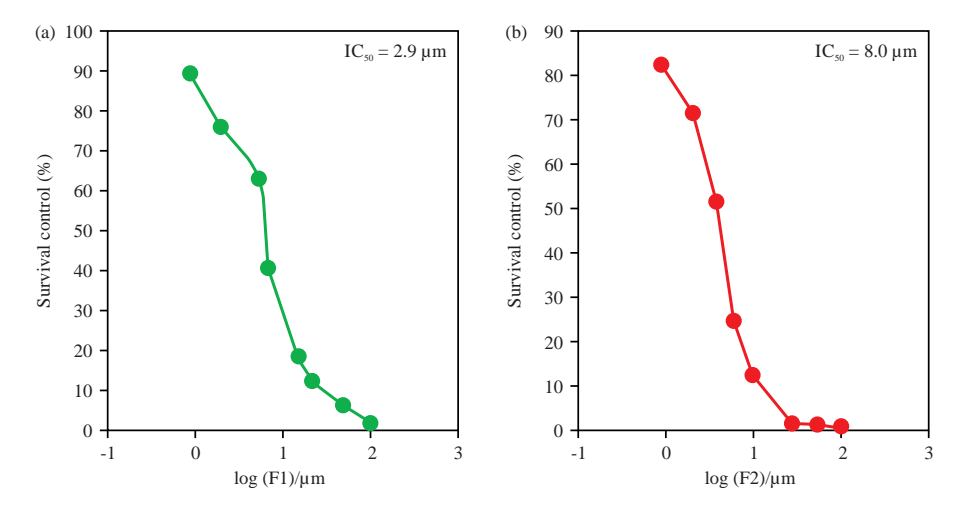


Fig. 5(a-b): Changes in survival rate of HepG2 tumor cells, (a-b) SR of HepG2 after F1 and F2 treatment for 48 hrs, respectively IC₅₀: Half-Maximal Inhibitory Concentration

Results of H&E staining in mouse liver and kidney: As displayed in Fig. 10(a-f) there were no discernible morphological alterations in the liver and kidney tissues of

mice following treatment. The size of cell nuclei was appropriately moderate, displaying intact shapes and uniform distribution of chromatin. This closely resembled the

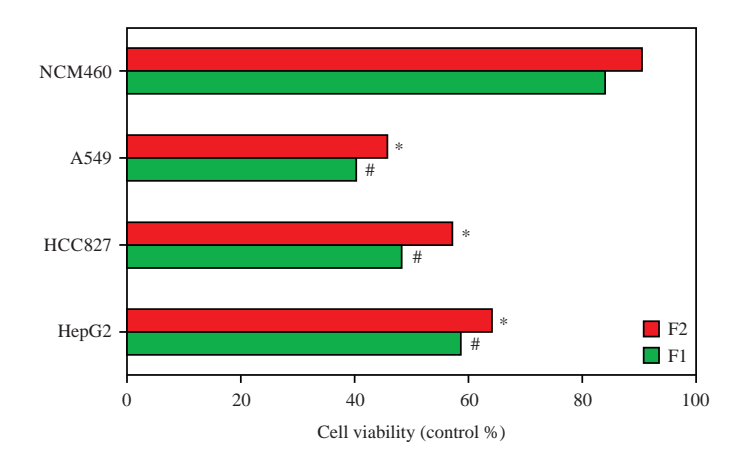


Fig. 6: SR of tumor cells after 24 hrs of F1 and F2 treatment

F1 treatment compared with SR without any treatment, p<0.05 and F2 treatment compared with SR without any treatment, p<0.05

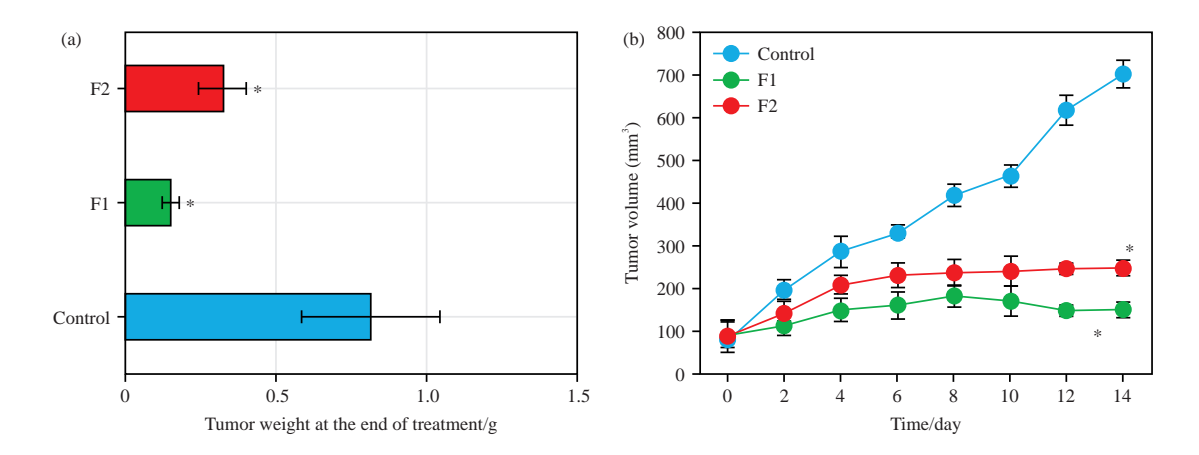


Fig. 7(a-b): Mouse xenograft experiment results, (a) Comparison of tumor tissue weights in mice after treatment completion across different groups and (b) Changes in tumor tissue volume in mice during the 14-day treatment period *Compared to the Ctrl group with p<0.001

morphology of liver and kidney tissues from the Ctrl group mice, indicating well-preserved cell structures without evident damage. These observations provide evidence that F1 and F2 can effectively inhibit the growth and development of tumor tissue, promote tumor cell apoptosis and concurrently exhibit lower toxicity to other normal cells, tissues and organs within the body.

DISCUSSION

Kinases are key PKs in cell signaling, playing crucial roles in regulating cellular processes such as growth, differentiation and apoptosis. Aberrant kinase activity is closely associated with the occurrence and progression of various tumors. Therefore, kinase inhibitors have garnered significant attention as an important class of anticancer drugs. Small

molecule kinase inhibitors, owing to their simple structure, good permeability and high bioavailability, have become one of the research hotspots in the field of cancer therapy.

Two small molecule kinase inhibitors, referred to as F1 and F2, were designed and evaluated for their impact on HCC827 and HepG2 cells. Flow cytometry analysis revealed a significant increase in the proportion of apoptotic cells within 48 hrs of F1 and F2 treatment, indicating a notable effect of these compounds on tumor cells. Annexin V, commonly used as a marker for detecting cell apoptosis in flow cytometry, was employed²². Cell apoptosis, a programmed cell death process, typically plays a vital role in normal development, tissue repair and maintaining cellular homeostasis. Annexin V binding to phosphatidylserine on the cell membrane enables rapid and reliable detection of cell apoptosis^{23,24}. Based on the staining status of Annexin V and another cell membrane marker

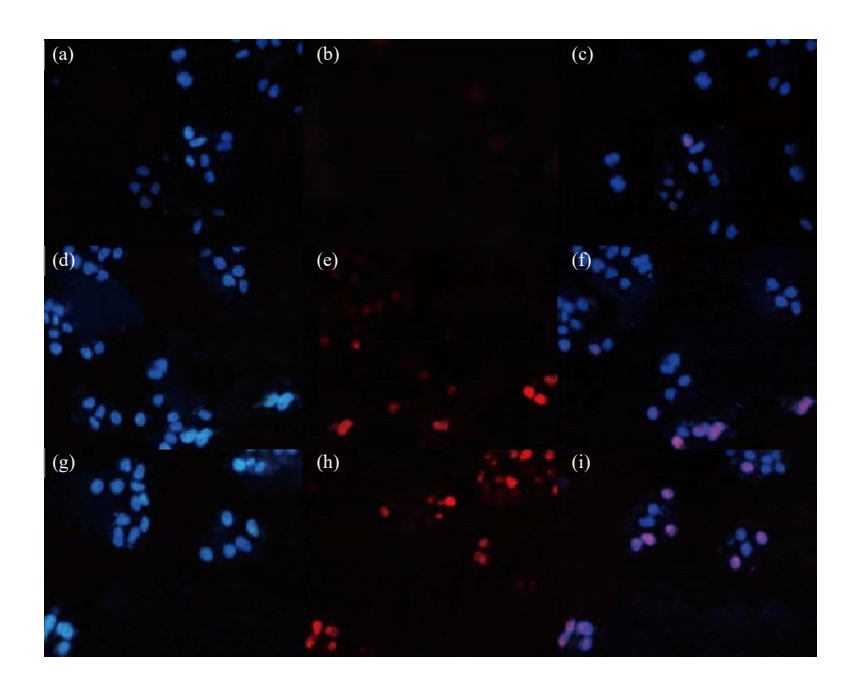


Fig. 8(a-i): Results of immunofluorescence staining, (a-c) γ H2AX, DAPI and Merged signals in Ctrl group, respectively, (d-f) γ H2AX, DAPI and Merged signals in F1 group, respectively and (g-i) γ H2AX, DAPI and Merged signals in F2 group, respectively

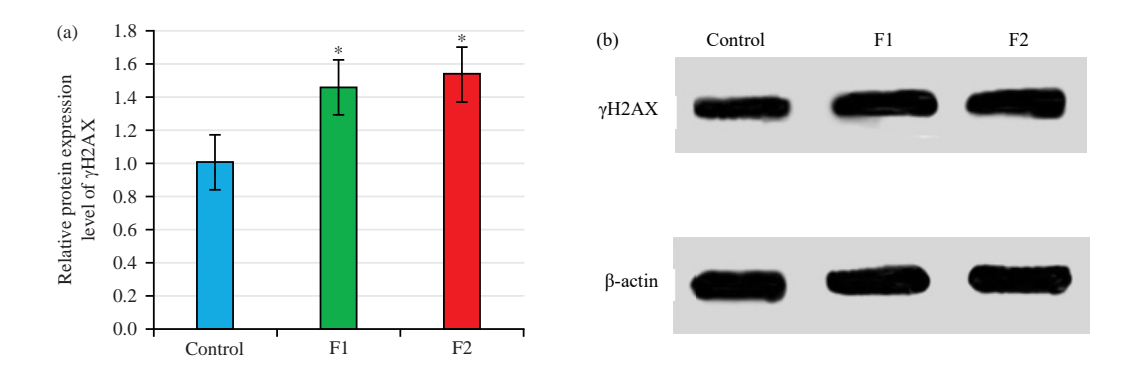


Fig. 9(a-b): Results of WB analysis conducted on tumor tissues, (a) Comparative results and (b) WB results *Compared to the Ctrl group with p<0.001

(such as PI), cells are classified into four distinct subgroups, including viable cells, early apoptotic cells, late apoptotic cells and necrotic or dead cells^{25,26}. The results indicated that F1 and F2 induced apoptosis in tumor cells after 24 hrs, achieving their anticancer effects. The MTT assay, a commonly used method to assess the cytotoxicity of compounds or samples, involves exposing cells to a yellow compound called MTT, which is then reduced by enzymes within metabolically active cells to form a blue formazan solution^{27,28}. By measuring the absorbance of the resulting blue product, cell viability and survival status can be evaluated. The IC_{50} (Half-Maximal Inhibitory Concentration) is a parameter used to assess the inhibitory effects of inhibitors or drugs on specific biological processes in the body. The IC_{50} value indicates the

concentration at which the compound can inhibit the biological process by 50%^{29,30}.

Further investigation revealed that the IC_{50} values of F1 and F2 against HepG2 tumor cells were 2.9 and 8.0 µm, respectively, both less than 10 µm. This suggests that F1 and F2 exhibit significant inhibitory effects on tumor cells and can exert potent biological activity at relatively low concentrations. Additionally, it was found that F1 and F2 exhibited varying degrees of cytotoxicity against A549, HCC827 and HepG2 cells, with cell viability significantly reduced after 24 hrs, remaining between 40-70%. This indicates that F1 and F2 possess selective cytotoxicity against tumor cells, while exhibiting less toxicity towards normal cells.

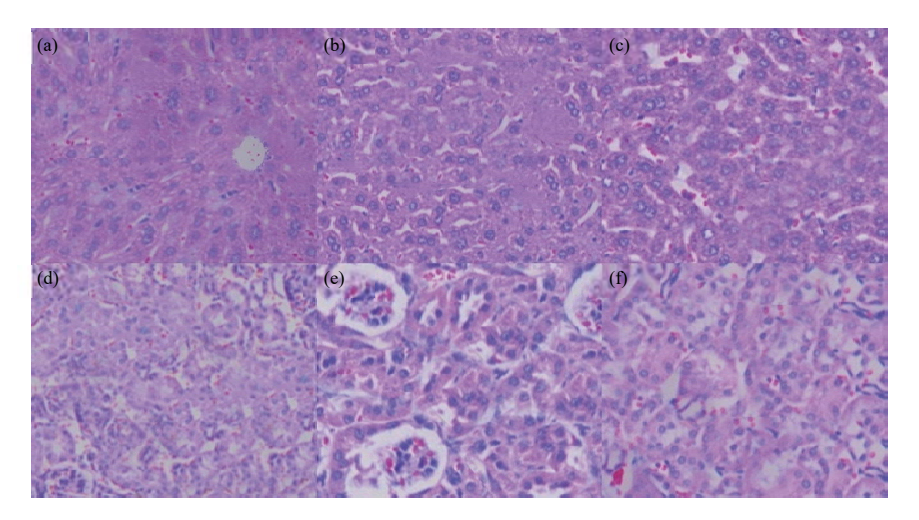


Fig. 10(a-f): Results of H&E staining in mouse liver and kidney (×400), (a-c) Liver sections of rats in Ctrl, F1 and F2 group after treatment, respectively and (d-f) Images for renal sections of rats in Ctrl, F1 and F2 group after intervention, respectively

This specificity may be attributed to the interaction of the compounds with specific biological targets within tumor cells, whereas these targets may be expressed at lower levels or involved in signal regulation of normal cell functions^{31,32}. The results indicated that F1 and F2 exhibited strong cytotoxic effects on tumor cells while exerting minimal cytotoxicity on normal cells. This suggests that these two compounds possess good selective toxicity in specific tumor cell lines.

The study further employed tumor model mice and through comparison, it was found that compared to the Ctrl group, both the tumor volume and weight of mice treated with F1 and F2 were significantly lower (p<0.001), indicating that F1 and F2 have similar inhibitory effects on the growth of live tumor tissues. Furthermore, immunofluorescence staining and immunoblot assays were conducted to detect the yH2AX signal and relative protein expression levels. The γH2AX signal serves as a marker of DNA damage, as cells initiate repair mechanisms in response to DNA damage, leading to phosphorylation of histone H2AX protein to form yH2AX. During this repair process, the ATM PK is activated and phosphorylates the H2AX protein, forming yH2AX^{33,34}. The yH2AX can form foci at the site of damage, aiding in cellular regulation and DNA repair^{35,36}. The results revealed that, compared to the Ctrl group, the γH2AX signal and relative protein expression levels of yH2AX in the F1 and F2 group were significantly elevated. Additionally, histological staining of liver and kidney tissues from mice using the Hematoxylin and Eosin (H&E) method showed no apparent morphological changes post-treatment. Cellular structures remained intact, devoid of evident damage. This suggests that F1 and F2, while inhibiting tumor tissue growth and

promoting tumor cell apoptosis, exhibit lower toxicity towards normal cells, tissues and organs *in vivo*. These findings indicate the potential anti-tumor activity of F1 and F2, coupled with favorable safety and tolerance profiles *in vivo*.

CONCLUSION

This research aimed to design, synthesize, optimize and evaluate the SMKIs for their anticancer activity. By thoroughly analyzing the structural characteristics of PKs, the PBC pharmacophore model was proposed, with special focus on two compounds, F1 and F2, that exhibited high tumorinhibitory potential. In cellular experiments, the MTT assay confirmed that both F1 and F2 extremely suppressed the tumor cell proliferation, while showing minimal impact on normal cells. This demonstrated a favorable tumor cellselective toxicity. Further experiments revealed that F1 had an IC_{50} of 2.9 µm and F2 had an IC_{50} of 8.0 µm, showcasing potent inhibitory activity. Through rat tumor xenograft experiments, this research further validated the inhibitory effects of F1 and F2 on *in vivo* tumor cells, with no apparent toxic side effects on rat liver and kidney tissues. This research suggested that the PBC pharmacophore model opened up new possibilities for the development of PK inhibitors in drug research. The F1 and F2, as representative compounds of this pharmacophore model, demonstrated promising anticancer activity and tumor cell-selective toxicity. They hold the potential for further development as anticancer drugs. In summary, this research yielded valuable insights into the design, synthesis, optimization and evaluation of SMKIs for their anticancer activity, paving the way for future research and drug development in this field.

SIGNIFICANCE STATEMENT

The study opened new avenues for the development of protein kinase inhibitors using PBC pharmacological models. The synthesized F1 and F2 compounds exhibit significant anti-tumor activity with minimal impact on normal cells, indicating significant tumor-selective toxicity. This achievement provides new prospects for drug design and optimization based on the model and is expected to bring new effective drugs for the treatment of diseases such as cancer.

REFERENCES

- Steinberg, G.R. and D. Carling, 2019. AMP-activated protein kinase: The current landscape for drug development. Nat. Rev. Drug Discovery, 18: 527-551.
- Borgo, C., C. D'Amore, S. Sarno, M. Salvi and M. Ruzzene, 2021. Protein kinase CK2: A potential therapeutic target for diverse human diseases. Signal Transduction Targeted Ther., Vol. 6. 10.1038/s41392-021-00567-7.
- Roskoski Jr., R., 2022. Properties of FDA-approved small molecule protein kinase inhibitors: A 2022 update. Pharmacol. Res., Vol. 175. 10.1016/j.phrs.2021.106037.
- 4. Chen, X., S. Chen and D. Yu, 2020. Protein kinase function of pyruvate kinase M2 and cancer. Cancer Cell Int., Vol. 20. 10.1186/s12935-020-01612-1.
- 5. Liang, S. and T.L. Blundell, 2023. Human DNA-dependent protein kinase activation mechanism. Nat. Struct. Mol. Biol., 30: 140-147.
- 6. He, S., Q. Li, Q. Huang and J. Cheng, 2022. Targeting protein kinase C for cancer therapy. Cancers, Vol. 14. 10.3390/cancers14051104.
- 7. Kanev, G.K., C. de Graaf, I.J.P. de Esch, R. Leurs, T. Würdinger, B.A. Westerman and A.J. Kooistra, 2019. The landscape of atypical and eukaryotic protein kinases. Trends Pharmacol. Sci., 40: 818-832.
- 8. Mifflin, L., D. Ofengeim and J. Yuan, 2020. Receptorinteracting protein kinase 1 (RIPK1) as a therapeutic target. Nat. Rev. Drug Discovery, 19: 553-571.
- Attwood, M.M., D. Fabbro, A.V. Sokolov, S. Knapp and H.B. Schiöth, 2021. Trends in kinase drug discovery: Targets, indications and inhibitor design. Nat. Rev. Drug Discovery, 20: 839-861.
- Li, M., Ashfaq Ur Rehman, Y. Liu, K. Chen and S. Lu, 2021. Dual Roles of ATP-Binding Site in Protein Kinases: Orthosteric Inhibition and Allosteric Regulation. In: Advances in Protein Chemistry and Structural Biology, Donev, R. (Ed.), Academic Press, Cambridge, Massachusetts, ISBN: 9780323853132, pp: 87-119.

- 11. Lu, X., J.B. Smaill and K. Ding, 2020. New promise and opportunities for allosteric kinase inhibitors. Angew. Chem. Int. Edn., 59: 13764-13776.
- 12. Pottier, C., M. Fresnais, M. Gilon, G. Jérusalem, R. Longuespée and N.E. Sounni, 2020. Tyrosine kinase inhibitors in cancer: Breakthrough and challenges of targeted therapy. Cancers, Vol. 12. 10.3390/cancers12030731.
- Xiang, H., J. Zhang, C. Lin, L. Zhang, B. Liu and L. Ouyang, 2020. Targeting autophagy-related protein kinases for potential therapeutic purpose. Acta Pharm. Sin. B, 10: 569-581.
- 14. Roskoski Jr., R., 2019. Small molecule inhibitors targeting the EGFR/ErbB family of protein-tyrosine kinases in human cancers. Pharmacol. Res., 139: 395-411.
- 15. Cohen, P., D. Cross and P.A. Jänne, 2021. Kinase drug discovery 20 years after imatinib: Progress and future directions. Nat. Rev. Drug Discovery, 20: 551-569.
- 16. Tian, X., K. Shoyama and Fr. Würthner, 2023. Nitrogen-doped polycyclic aromatic hydrocarbons by a one-pot Suzuki coupling/intramolecular S_NAr reaction. Chem. Sci., 14: 284-290.
- 17. Zhang, Y.Y., J.X. Li, L.L. Ding, L. Liu, S.M. Wang and Z.B. Han, 2018. Palladium nanoparticles encapsulated in the MIL-101-catalyzed one-pot reaction of alcohol oxidation and aldimine condensation. Inorg. Chem., 57: 13586-13593.
- 18. Mayer, L., R. Kohlbecher and T.J.J. Müller, 2020. Concatenating Suzuki arylation and Buchwald-Hartwig amination by a sequentially Pd-catalyzed one-pot process-consecutive three-component synthesis of *C,N*-diarylated heterocycles. Chem. A Eur. J., 26: 15130-15134.
- Li, X., T. Zhang, R. Hu, H. Zhang, C. Ren and Z. Yuan, 2020.
 A one-pot protocol for the fluorosulfonation and Suzuki coupling of phenols and bromophenols, streamlined access to biaryls and terphenyls. Org. Biomol. Chem., 18: 4748-4753.
- 20. Wang, C., Y.C. Liu, M.Y. Xu and B. Xiao, 2021. Synthesis of dialkyl-substituted monofluoroalkenes via palladium-catalyzed cross-coupling of alkyl carbagermatranes. Org. Lett., 23: 4593-4597.
- Ilaghi, M., I. Sharifi, F. Sharififar, F. Sharifi and R.T. Oliaee et al., 2021. The potential role and apoptotic profile of three medicinal plant extracts on *Leishmania tropica* by MTT assay, macrophage model and flow cytometry analysis. Parasite Epidemiol. Control, Vol. 12. 10.1016/j.parepi.2021.e00201.
- Gobin, C.M., J.N. Menefee, C.C. Lattimore, A. Doty and K.M. Fredenburg, 2022. Cell dissociation enzymes affect annexin V/flow-cytometric apoptotic assay outcomes after miRNA-based transient transfection. Anticancer Res., 42: 2819-2825.
- Ostermann, M., A. Sauter, Y. Xue, E. Birkeland, J. Schoelermann, B. Holst and M.R. Cimpan, 2020. Label-free impedance flow cytometry for nanotoxicity screening. Sci. Rep., Vol. 10. 10.1038/s41598-019-56705-3.

- 24. Daddiouaissa, D., A. Amid, N.A. Kabbashi, F.A.A. Fuad, A.A.M. Elnour and M.A.K.M.S. Epandy, 2019. Antiproliferative activity of ionic liquid-graviola fruit extract against human breast cancer (MCF-7) cell lines using flow cytometry techniques. J. Ethnopharmacol., 236: 466-473.
- Barani, M., M. Mirzaei, M. Torkzadeh-Mahani and M. Adeli-Sardou, 2019. Evaluation of carum-loaded niosomes on breast cancer cells: Physicochemical properties, *in vitro* cytotoxicity, flow cytometric, DNA fragmentation and cell migration assay. Sci. Rep., Vol. 9. 10.1038/s41598-019-43755-w.
- Li, Y., H. Zang, G. Qian, T.K. Owonikoko, S.R. Ramalingam and S.Y. Sun, 2020. ERK inhibition effectively overcomes acquired resistance of epidermal growth factor receptormutant non-small cell lung cancer cells to osimertinib. Cancer, 126: 1339-1350.
- 27. Mairuae, N., N. Palachai and P. Noisa, 2024. An anthocyanin-rich extract from *Zea mays* L. *var. ceratina* alleviates neuronal cell death caused by hydrogen peroxide-induced cytotoxicity in SH-SY5Y cells. BMC Complementary Med. Ther., Vol. 24. 10.1186/s12906-024-04458-6.
- 28. Kumar, A., S. Kour, S. Kaul, A. Malik, R. Dhani and R. Kaul, 2023. Cytotoxicity evaluation of Bio-C, CeraSeal, MTA-Fillapex, and AH Plus root canal sealers by microscopic and 3-(4, 5 dimethythiazol-2yl)-2, 5-diphenyltetrazolium bromide (MTT) assay. J. Conservative Dent., 26: 73-78.
- Chakravorty, A., V. Ravindran, G. Jeevanandan and A. Arthanari, 2023. The cytotoxic assessment of antibacterial-enhanced mineral trioxide aggregate compared to commercially available bioceramic cements by using methyl-thiazoldiphenyl-tetrazolium (MTT) assay on human dental pulp stem cells: An *in vitro* study. Cureus, Vol. 15. 10.7759/cureus.49691.

- Ghasemi, M., T. Turnbull, S. Sebastian and I. Kempson, 2021.
 The MTT assay: Utility, limitations, pitfalls, and interpretation in bulk and single-cell analysis. Int. J. Mol. Sci., Vol. 22. 10.3390/ijms222312827.
- 31. Abdel-Maksoud, M.S., R.M. Hassan, A.A.S. El-Azzouny, M.N. Aboul-Enein and C.H. Oh, 2021. Anticancer profile and anti-inflammatory effect of new *N*-(2-((4-(1,3-diphenyl-*1H*-pyrazol-4-yl))pyridine sulfonamide derivatives. Bioorg. Chem., Vol. 117. 10.1016/j.bioorg.2021.105424.
- 32. Wu, S.Y., T. Fu, Y.Z. Jiang and Z.M. Shao, 2020. Natural killer cells in cancer biology and therapy. Mol. Cancer, Vol. 19. 10.1186/s12943-020-01238-x.
- 33. Kopp, B., L. Khoury and M. Audebert, 2019. Validation of the γ H2AX biomarker for genotoxicity assessment: A review. Arch. Toxicol., 93: 2103-2114.
- 34. Valente, D., M.P. Gentileschi, A. Guerrisi, V. Bruzzaniti, A. Morrone, S. Soddu and A. Verdina, 2022. Factors to consider for the correct use of γH2AX in the evaluation of DNA double-strand breaks damage caused by ionizing radiation. Cancers, Vol. 14. 10.3390/cancers14246204.
- 35. Hahn, H., C. Neitzel, O. Kopečná, D.W. Heermann, M. Falk and M. Hausmann, 2021. Topological analysis of γH2AX and MRE11 clusters detected by localization microscopy during X-ray-induced DNA double-strand break repair. Cancers, Vol. 13. 10.3390/cancers13215561.
- 36. Lyu, X., M. Chastain and W. Chai, 2019. Genome-wide mapping and profiling of γ H2AX binding hotspots in response to different replication stress inducers. BMC Genomics, Vol. 20. 10.1186/s12864-019-5934-4.